HHS Public Access

Author manuscript

Cell Rep. Author manuscript; available in PMC 2017 February 19.

Published in final edited form as:

Cell Rep. 2016 August 09; 16(6): 1561–1573. doi:10.1016/j.celrep.2016.07.011.

MICU1 serves as a molecular gatekeeper to prevent *in vivo* mitochondrial calcium overload

Julia C. Liu[1], **Jie Liu**[1], **Kira M. Holmström**[1], **Sara Menazza**[2], **Randi J. Parks**[2], **Maria M. Fergusson**[1], **Zu-Xi Yu**[3], **Danielle A. Springer**[4], **Charles Halsey**[5], **Chengyu Liu**[6], **Elizabeth Murphy**[2], and **Toren Finkel**[1]

[1]) Center for Molecular Medicine, NHLBI, NIH, Bethesda, MD 20892 USA

[2]) Systems Biology Center, NHLBI, NIH, Bethesda, MD 20892 USA

[3]) Pathology Core, NHLBI, NIH, Bethesda, MD 20892 USA

[4]) Murine Phenotyping Core, NHLBI, NIH, Bethesda, MD 20892 USA

[5]) Laboratory of Cancer Biology and Genetics, NCI, NIH, Bethesda, MD 20892 USA

[6]) Transgenic Core, NHLBI, NIH, Bethesda, MD 20892 USA

Abstract

MICU1 is a component of the mitochondrial calcium uniporter, a multiprotein complex that also includes MICU2, MCU, and EMRE. Here, we describe a mouse model of MICU1 deficiency. MICU1$^{-/-}$ mitochondria demonstrate altered calcium uptake and deletion of MICU1 results in significant, but not complete, perinatal mortality. Similar to afflicted patients, viable MICU1$^{-/-}$ mice manifest marked ataxia and muscle weakness. Early in life, these animals display a range of biochemical abnormalities including increased resting mitochondrial calcium levels, altered mitochondrial morphology, and reduced ATP. Older MICU1$^{-/-}$ mice show marked, spontaneous improvement, coincident with improved mitochondrial calcium handling and an age-dependent reduction in EMRE expression. Remarkably, deleting one allele of EMRE helps normalize calcium uptake while simultaneously rescuing the high perinatal mortality observed in young MICU1$^{-/-}$ mice. Together, these results demonstrate that MICU1 serves as a molecular gatekeeper preventing calcium overload and suggests that modulating the calcium uniporter could have widespread therapeutic benefits.

Abstract

Address Correspondence: Toren Finkel MD/PhD, Center for Molecular Medicine, Bldg 10/CRC 5-3330, 10 Center Drive, Bethesda, MD 20892 USA, T: 301-402-4081, Fax: 301-402-088, finkelt@nih.gov.

Supplemental Information: Supplemental information includes Supplemental Experimental Procedures and six Supplemental Figures.

Author Contribution: J.C.L., J.L., K.M.H., S.M, R.J.P and M.M.F. performed the experiments, Z.Y and C.H. helped with the pathological analysis, D.A.S. performed the neurological and skeletal muscle phenotyping, C.L. constructed the mouse models, E.M. and T.F conceived the project. J.C.L. and T.F. wrote the manuscript.

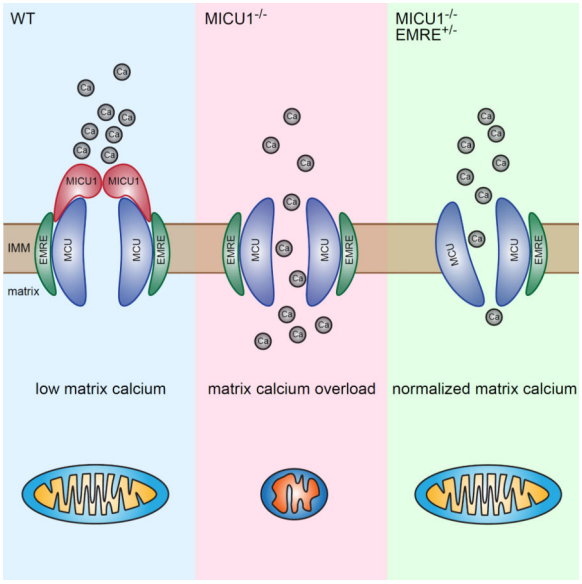

Introduction

Calcium entry into the mitochondria is critical for cellular homeostasis and is believed to modulate bioenergetic capacity and help determine the threshold for cell death (Balaban, 2009; Orrenius et al., 2003). For over fifty years, it has been appreciated that isolated mitochondria could rapidly take up calcium, using the large mitochondrial membrane potential across the inner mitochondrial membrane as a driving force for the entry of the ion (Deluca and Engstrom, 1961; Vasington and Murphy, 1962). Subsequent studies demonstrated that this uptake was highly selective for calcium (Kirichok et al., 2004). These and other studies help define the biophysical properties of the inner mitochondrial membrane channel now termed the mitochondrial calcium uniporter complex. Nonetheless, the molecular components of the uniporter complex remained elusive for over five decades. However, in the last several years, rapid progress has been made, including the molecular identification of a 40 kD inner mitochondrial membrane protein (MCU) as the pore forming protein of the uniporter complex (Baughman et al., 2011; De Stefani et al., 2011).

The composition of the uniporter complex is now believed to contain several additional components beyond the pore-forming MCU protein. These include the MCU paralog MCUb, a family of related EF-hand containing proteins MICU1, MICU2, and MICU3, and a small 10 kD protein EMRE (Foskett and Philipson, 2015; Kamer and Mootha, 2015; Murgia and Rizzuto, 2015). The composition of the uniporter complex appears to differ between various cell lines and between different tissues, as for instance the expression of MICU3 appears largely confined to the brain (Plovanich et al., 2013), and the relative ratio of MCU and MCUb appears to markedly differ in various organs (Raffaello et al., 2013). These differences in composition might, in turn, be important for the observed tissue-specific differences in uniporter activity (Fieni et al., 2012).

While the recent molecular identification of MCU has provided significant insight into the regulation of mitochondrial calcium entry, numerous questions persist. Experimental evidence suggests that rates of calcium entry through the uniporter are sigmoidal, with slow rates of calcium uptake at low extra-mitochondrial calcium concentrations, and faster uptake when calcium concentrations begin to exceed 10–15 μM (Csordas et al., 1999; Csordas et al., 2010; Giacomello et al., 2010; Rizzuto et al., 1998). This sigmoidal behavior is critical, as this endows resistance to calcium overload at resting cytosolic calcium levels, while still allowing the mitochondria to respond to a rise in cytoplasmic calcium induced by agonist stimulation. While such gating behavior could result from the intrinsic properties of MCU itself, considerable attention has focused on other components of the uniporter complex. Particular emphasis has been placed on what inhibits calcium uptake at low calcium levels, providing the necessary gatekeeping functions of the uniporter, and thus preventing the potentially disastrous consequences of calcium overload. Studies have suggested that both MICU1 (Csordas et al., 2013; de la Fuente et al., 2014; Kamer and Mootha, 2014; Mallilankaraman et al., 2012) and MICU2 (Patron et al., 2014) might mediate this gatekeeping function. To date, most studies have relied on the behavior of permeabilized cell lines, in which uniporter components were knocked down (Csordas et al., 2013; de la Fuente et al., 2014; Mallilankaraman et al., 2012; Patron et al., 2014), or using specific cell lines containing CRISPR-mediated cellular knockouts (Kamer and Mootha, 2014). Analysis of this cellular data employing knockdown and knockout of MICU1 has, however, often revealed conflicting results. For instance, the role of MICU1 at high calcium concentrations has varied between studies, with some arguing that knockdown of MICU1 does not alter mitochondrial calcium uptake following agonist-induced calcium release (Mallilankaraman et al., 2012). Others have suggested that cells lacking MICU1 are impaired in this capacity (Csordas et al., 2013; Perocchi et al., 2010), while still others have demonstrated that the effects may be determined by the strength of the agonist stimulation (de la Fuente et al., 2014). There are similar ambiguities with regard to whether genetic inhibition of MICU1 leads to resting calcium overload, again with some studies arguing it does (Mallilankaraman et al., 2012; Patron et al., 2014) and others suggesting it does not (Csordas et al., 2013; de la Fuente et al., 2014; Perocchi et al., 2010). It is likely that differences in experimental approaches, including differences in the degree of knockdown, as well as differences in the intrinsic composition of the uniporter complex in the various cell lines employed, might at least partially explain these divergent results.

Further insight into the regulation of uniporter activity has come from the recent description of a cohort of children who presented with a range of severe symptoms characterized by profound proximal skeletal muscle weakness, accompanied by neurological features that included chorea, tremors, and ataxia (Logan et al., 2014). Subsequent genetic analysis identified the afflicted children carried loss-of-function mutations in MICU1 that were inherited in an autosomal recessive fashion. Initial characterization of fibroblast cell lines derived from patients and controls were consistent with the hypothesis that loss of MICU1 leads to mitochondrial calcium overload (Logan et al., 2014). While MICU1 deficiency is rare, the clinical phenotype described in these patients shares features with other more common conditions including muscular dystrophies, as well as congenital and mitochondrial myopathies. These entities are often accompanied by mitochondrial dysfunction and

damage. Indeed, mitochondrial calcium overload is being increasingly viewed as a common final pathway for a wide range of human pathologies (Abeti and Abramov, 2015; Bhosale et al., 2015; Martin and McGee, 2014; Santulli et al., 2015; Vallejo-Illarramendi et al., 2014). Most of these conditions, like MICU1 deficiency, have few therapeutic options.

Here, we describe a mouse model in which we have deleted MICU1. These mice exhibit many of the characteristics recently observed in patients lacking MICU1 expression. Remarkably, while the absence of MICU1 leads to high perinatal mortality and marked abnormalities in young mice, many, but not all, of these defects improve with time. Older MICU1$^{-/-}$ mice also have improved mitochondrial calcium handling parameters, suggesting an age-dependent remodeling of their uniporter complex. Consistent with this remodeling, older MICU1$^{-/-}$ mice demonstrate a decline in EMRE expression. To further assess the importance of this decline in EMRE expression, we generated mice with targeted deletions in the EMRE locus. Surprisingly, EMRE heterozygosity significantly ameliorates the MICU1$^{-/-}$ phenotype. As such, these results clarify the molecular regulation of mitochondrial calcium influx and suggest potential strategies that might have therapeutic benefit in the growing number of conditions characterized by calcium overload.

Results

MICU1 deletion alters calcium uptake rates

In an effort to better understand the molecular function of MICU1, we generated MICU1$^{-/-}$ mice using CRISPR-mediated methods. Four different founder mice, representing four independent genomic targeting events, were generated (Figure S1A). Each line yielded similar results and as such, we have incorporated data from all four lines. As expected, mitochondria isolated from this MICU1$^{-/-}$ mouse lacked expression of MICU1 protein (Figure S1B). We next asked whether deletion of MICU1 altered calcium uptake. Wild-type (WT) liver mitochondria loaded with a calcium-sensitive fluorophore showed little evidence of calcium uptake when challenged with a low concentration (estimated free calcium concentration of 0.5 μM) of extra-mitochondrial calcium (Figure 1A). In contrast, the absence of MICU1 expression led to a significantly increased rate of calcium uptake under these conditions (Figure 1A and 1B). In the setting of higher concentrations of extra-mitochondrial calcium (estimated free calcium concentration of 16 μM), the absence of MICU1 appeared to reduce the rate of mitochondrial calcium entry (Figure 1C and 1D). Similar alterations in calcium uptake were observed in MICU1$^{-/-}$ mitochondria isolated from other tissues such as brain (Figure S1C and S1D). Thus, in purified mitochondria, the absence of MICU1 expression augments calcium uptake rates at low calcium concentrations, and inhibits uptake rates at high calcium concentrations.

We further validated these properties using mouse embryonic fibroblasts (MEFs) derived from embryos of MICU1$^{-/-}$ mice or their WT littermates. As observed in isolated mitochondria, MICU1$^{-/-}$ MEFs lacked discernable MICU1 expression (Figure 1E). As seen with isolated mitochondria, permeabilized WT MEFs showed little uptake of calcium at low calcium concentrations (Figure 1F). In contrast to WT MEFs, MICU1$^{-/-}$ MEFs displayed increased rates of calcium uptake under these same conditions (Figure 1F and 1G). When

MICU1 expression was reconstituted in MICU1-deficient cells (Figure 1E), WT calcium uptake properties were restored (Figure 1F and 1G).

MICU1$^{-/-}$ mice develop severe neurological and myopathic defects

We next sought to characterize the phenotype of mice lacking MICU1 expression. Breeding of heterozygous MICU1$^{+/-}$ resulted in significantly fewer MICU1$^{-/-}$ mice than expected. Analysis of over 1300 births demonstrated that only one in roughly every six or seven MICU1$^{-/-}$ animals were able to survive beyond the first postnatal week (Figure 2A). In contrast, examination of litters from late embryogenesis to immediately after birth demonstrated that while late-stage MICU1$^{-/-}$ embryos were slightly smaller than WT littermates (Figure 2B), there appeared to be no embryonic selection against MICU1$^{-/-}$ progeny. Indeed, when we analyzed a total of 60 late stage embryos/P1 pups, we observed the precise number of mice expected in each genotype (15 WT, 30 MICU1$^{+/-}$ and 15 MICU1$^{-/-}$ mice, equivalent to a 25% frequency of knockouts). In contrast, while it is not unusual for some pups to die in the first few days after birth, when we assessed the litters of MICU1$^{+/-}$ crosses, 96 out of 138 spontaneous perinatal deaths (70%) were of the MICU1$^{-/-}$ genotype. Thus, while MICU1 expression appears largely dispensable for development, the absence of MICU1 results in a high, but not complete, perinatal death rate. These observations contrast slightly from a very recent report demonstrating that MICU1 deletion resulted in 100% perinatal mortality (Antony et al., 2016). In that report, the authors observed that MICU1$^{-/-}$ mice exhibited decreased number of specific brainstem neurons known to regulate respiration. While this decrease was just a trend, other models where deletion of critical mitochondrial proteins leads to perinatal mortality have also shown impaired neuronal innervation of the diaphragm (Nguyen et al., 2014). In that context, we also observed a modest trend for a decreased number of cervical motor neurons required for respiration in MICU1$^{-/-}$ late-term embryos (Figure S2A and S2B), although it remains unclear to what degree this contributed to the high rate of perinatal death.

At one week of age, surviving MICU1$^{-/-}$ mice appeared underdeveloped, smaller and weighed roughly 50% less than their WT littermates (Figure 2C and 2D). Young MICU1$^{-/-}$ mice, like children bearing mutations in MICU1, appear to suffer from ataxia. Functional analysis revealed that one month old MICU1$^{-/-}$ mice had severely impaired performance on a balance beam (Figure 2E). A closer histological examination of the cerebellum revealed abnormal persistence of the outer granular layer in 12-day-old mice lacking MICU1 expression (Figure 2F and 2G). In addition, the overall cerebellum of young MICU1$^{-/-}$ mice appeared underdeveloped (Figure S2C). Consistent with their observed neurological defects, MICU1$^{-/-}$ mice also exhibited alterations in the postnatal arborization of Purkinje cells (Figure 2H and 2I). Given that patients lacking MICU1 develop proximal myopathies, we also assessed muscle strength in MICU1$^{-/-}$ mice. Histologically, we did not observe any evidence of central nuclei, or marked changes in the abundance of fast and slow fibers in the skeletal muscle of MICU1$^{-/-}$ mice (Figure S2D–S2F). Similarly, histochemical enzyme assays of succinate dehydrogenase (SDH) and cytochrome c oxidase (COX) activity revealed no significant differences between WT and MICU1$^{-/-}$ muscle fibers, except that, consistent with overall body size, the MICU1$^{-/-}$ fibers were considerably smaller (Figure S2G and S2H). Nonetheless, 4-week-old MICU1$^{-/-}$ mice were markedly impaired in an

inverted grid test of skeletal muscle function (Figure 2J), as well as in their performance in a wire hang test, another measure of skeletal muscle strength and coordination (Figure S2I). Thus, these mice appear to exhibit many of the neurological and myopathic defects observed in MICU1-deficient patients. We also, however, observed additional properties not formally assessed in human patients. While analysis of splenic and thymic T cell maturation revealed no discernable alterations (Figure S3A–S3F), the numbers of splenic B cells were markedly reduced in MICU1$^{-/-}$ mice (Figure 2K–M and Figure S3G–I). This decrease in overall B cell number was consistent with an observed increase in cell death observed in MICU1$^{-/-}$ B cells (Figure S3J–L). The more pronounced effects observed in B cells, when compared to T cells, may reflect intrinsic differences in MICU1 expression between these two cell types (Figure S3M).

MICU1 deletion leads to calcium overload

We next sought to better understand the biochemical basis underlying the various phenotypic alterations observed in MICU1$^{-/-}$ mice. Given our observations that depending on the calcium concentration, MICU1 deletion has either positive or negative effects on calcium uptake, the net effect on resting mitochondrial calcium levels was difficult to *a priori* predict. Therefore, we first sought to directly measure *in situ* matrix mitochondrial calcium levels. This analysis revealed that mitochondria from young MICU1$^{-/-}$ mice had an approximate 1.5-fold increase in their resting levels of mitochondrial matrix calcium (Figure 3A). This argues that the predominant *in vivo* effect of MICU1 is to function as a gatekeeper, as in the absence of this molecule, mitochondria exhibit tonic calcium overload. A number of abnormalities have previously been associated with calcium overload, including alterations in mitochondrial morphology and increased generation of reactive oxygen species (ROS) (Peng and Jou, 2010). Consistent with these past observations in other systems, electron micrographs revealed MICU1$^{-/-}$ mice had marked alterations in skeletal muscle mitochondrial morphology (Figure 3B and 3C). Similar alterations were seen with mitochondria in the brain (Figure S4A). In addition, we noted that ATP levels were also significantly reduced in MICU1$^{-/-}$ skeletal muscle (Figure 3D), although alterations in resting ATP levels were not as evident in the brain (Figure S4B). A further common hallmark of mitochondrial dysfunction is a rise in lactate levels, a feature also evident in the skeletal muscle of MICU1$^{-/-}$ mice (Figure 3E). We saw a similar increase in blood lactate levels (Figure S4C). To assess tissue ROS levels, we took advantage of our previous observations of B cell defects in MICU1$^{-/-}$ mice (Figure 2M). Using the redox-sensitive fluorophore DCFDA, we noted a significant increase in the ROS levels observed in MICU1$^{-/-}$ B cells (Figure 3F and 3G). A similar elevation in ROS levels was also seen in thymic-derived T cells (Figures S4D and 4E). Mitochondrial uncoupling abrogated the difference in ROS levels between WT and MICU1$^{-/-}$ cells, consistent with a mitochondrial source for the elevated levels of ROS observed in MICU1$^{-/-}$ cells (Figure S4F and S4G).

Age-dependent improvement in MICU1$^{-/-}$ mice

While the survival and appearance of newborn and young MICU1$^{-/-}$ mice was markedly impaired, we noted that surviving MICU1$^{-/-}$ mice appeared to improve over time (Figure 4A). This improvement was evident in appearance and overall body weight. While MICU1$^{-/-}$ mice remained smaller than their WT littermates, these differences narrowed

considerably as the animals aged (Figure 4B). With this phenotypic improvement, we noted that differences in resting calcium, ATP, and muscle lactate were no longer significantly different between older WT and MICU1$^{-/-}$ mice, although a trend towards increased resting calcium, decreased resting ATP, and increased lactate remained (Figure 4C–E). Similarly, the differences in B cell abundance and ROS levels observed in young MICU1$^{-/-}$ mice were no longer evident as these animals aged (Figure 4F–H and Figure S5A–C). Histological assessment of the cerebellum of MICU1$^{-/-}$ mice revealed that previous abnormalities such as a persistent outer granular layer resolved in the brains of older MICU1$^{-/-}$ mice (Figure 4I and 4J). This suggests that MICU1$^{-/-}$ mice experience a developmental delay, rather than a complete block, of this post-natal cerebellar process. While many of the histological and biochemical parameters improved in the older MICU1$^{-/-}$ mice, we did however continue to see persistent functional defects in both neurological and skeletal muscle function (Figure S5D and S5E). In addition, as these animals age, new abnormalities arose. For instance, electron micrographs of skeletal muscle revealed the presence of tubular aggregates (Figure 4K). Interestingly, in humans, this relatively rare myopathic abnormality has been recently described to result from alterations in skeletal muscle calcium handling due to patients inheriting dominant mutations in stromal interaction molecule 1 (STIM1), an ER calcium sensor (Bohm et al., 2013).

In an effort to explain why some of the parameters improved in MICU1$^{-/-}$ mice as they aged, we reevaluated calcium uptake parameters from mitochondria derived from the liver of older MICU1$^{-/-}$ animals. While the defects in calcium uptake at high calcium concentrations remained essentially unchanged (Figure S5F and S5G), we noted that the loss of gatekeeping function at low calcium concentrations was now less marked (Figure 5A and 5B; compare to Figure 1A). This suggested that some age-dependent remodeling of the uniporter complex might have occurred. We therefore examined the levels of MCU and EMRE proteins in the liver of young (2-week-old) and old (7-month-old) WT and MICU1$^{-/-}$ mice. We noted that at 2 weeks of age, surviving MICU1$^{-/-}$ animals had similar levels of MCU as WT animals, but had a reduced EMRE to MCU expression ratio (Figure 5C). Interestingly, at seven months of age, the EMRE/MCU expression ratio had fallen even lower in these now, phenotypically improved, older MICU1$^{-/-}$ mice.

EMRE heterozygosity rescues MICU1$^{-/-}$ mice

Previous observations with EMRE knockdown in cultured cells suggest that EMRE functions as a scaffold for MCU and is required to maintain channel opening (Kovacs-Bogdan et al., 2014; Sancak et al., 2013; Vais et al., 2016). Our observation that reduced expression of EMRE in older MICU1$^{-/-}$ mice correlated with phenotypic improvement suggested that MICU1$^{-/-}$ mice might remodel their uniporter complex by reducing EMRE expression. Such remodeling would likely limit uniporter opening and hence help prevent calcium entry and *in vivo* calcium overload. To test this hypothesis, we reasoned that genetically reducing EMRE expression might therefore provide a benefit in the setting of MICU1 deficiency. Using CRISPR-mediated methods, we therefore generated additional mice containing targeted deletions in the EMRE locus located on chromosome 15 of the mouse (Figure S6A). We crossed MICU1$^{+/-}$EMRE$^{+/-}$ mice to ask whether EMRE deficiency could rescue the perinatal mortality of MICU1$^{-/-}$ mice. As expected, only a small

fraction of MICU1$^{-/-}$EMRE$^{+/+}$ mice survived into the first week (Figure 6A). Similarly, to date, we have not observed any surviving MICU1$^{-/-}$EMRE$^{-/-}$ mice; however, in this mixed genetic background, we were able to generate MICU1$^{+/+}$EMRE$^{-/-}$ mice (Figure S6B). Mice lacking EMRE but having wild-type MICU1 appeared to have normal body weights, and exhibited no evidence of ataxia or defects in skeletal muscle function (Figure S6C–E).

Remarkably, MICU1$^{-/-}$ EMRE$^{+/-}$ mice were observed at nearly the expected frequency at weaning (Figure 6A). We saw a similar capacity to rescue MICU1-deficient animals using a second, independent, CRISPR-generated EMRE-deficient mouse line (Figure S6A). Interestingly, young MICU1$^{-/-}$ EMRE$^{+/-}$ mice had reduced hepatic levels of EMRE expression compared to MICU1$^{-/-}$ mice (Figure 6B). The overall appearance and weight of the MICU1$^{-/-}$ EMRE$^{+/-}$ mice was indistinguishable from WT mice (Figure 6C and Figure S6F). Based on this genetic rescue, we next asked whether in the context of MICU1 deletion, deleting one allele of EMRE resulted in improved calcium uptake. We observed that liver mitochondria from young MICU1$^{-/-}$ EMRE$^{+/-}$ mice still had slightly impaired gatekeeping function at low extra-mitochondrial calcium levels (Figure 6D). Under these low calcium conditions, MICU1$^{-/-}$ EMRE$^{+/-}$ mitochondria had roughly 2-fold higher rates of calcium uptake than WT mitochondria (Figure 6E). Nonetheless, this defect was markedly reduced when compared to the nearly 6-fold difference previously observed in MICU1$^{-/-}$ mitochondria (see Figure 1B). At high calcium concentrations, a situation in which MICU1$^{-/-}$ mitochondria demonstrate reduced rates of calcium uptake, EMRE heterozygosity resulted in a modest but further reduction in this property (Figure 6F and 6G, compare to Figure 1D). These results are consistent with a role for EMRE in maintaining channel opening, as in the absence of MICU1 expression, deletion of one allele of EMRE reduced EMRE expression and resulted in reduced calcium uptake at both low and high extra-mitochondrial calcium levels. Interestingly, by itself, EMRE heterozygosity appeared to have no significant effect on hepatic EMRE levels or on calcium uptake (Figure S6G–I). This suggests that in the setting of wild-type levels of the other uniporter complex components, one allele of EMRE is sufficient to maintain the required level of protein expression. We cannot however exclude the possibility that the reason the effects of deleting one allele of EMRE is only evident in the context of MICU1 deletion relates to the recent observation that EMRE's activity can be regulated by a rise in matrix calcium levels (Vais et al., 2016), a situation that presumably occurs in MICU1$^{-/-}$, but not WT, mitochondria.

Consistent with the observed reduction in calcium uptake at low calcium levels, brain matrix calcium levels appeared similar between WT and MICU1$^{-/-}$ EMRE$^{+/-}$ mitochondria isolated from young mice (Figure 6H, compare to Figure 3A). Skeletal muscle mitochondrial morphology was also apparently normalized in these mice (Figure 6I). Similarly, while skeletal muscle ATP levels trended slightly lower than seen in WT mice, this difference was not statistically significant (Figure 6J, compare to Figure 3D). Young MICU1$^{-/-}$ EMRE$^{+/-}$ animals also exhibited age-appropriate cerebellar morphology (Figure 6K) and an amelioration of the observed B cell alterations (Figures S6J–O). Moreover, when compared to MICU1$^{-/-}$ mice (Figure 2E), MICU1$^{-/-}$ EMRE$^{+/-}$ mice exhibited improvement in their performance on the balance beam, although they were still impaired when compared to WT animals (Figure 6L). Similarly, skeletal muscle strength was still impaired in the

MICU1$^{-/-}$ EMRE$^{+/-}$ mice, although again, these animals performed slightly better than MICU1$^{-/-}$ animals (Figure S6P).

Discussion

Our results significantly clarify the *in vivo* function of MICU1. In particular, using isolated WT and MICU1$^{-/-}$ mitochondria, we demonstrate that the absence of MICU1 increases mitochondrial calcium uptake rates at low calcium concentrations and reduces calcium entry rates at high calcium concentrations. Nonetheless, while these changes in gating properties could theoretically lead to either increased or decreased mitochondrial calcium levels, our data suggest that *in vivo*, the primary function of MICU1 is to function as a molecular gatekeeper. In particular, in the absence of MICU1, mitochondrial matrix calcium levels are increased, and the deleterious consequences of this increase are evident in a wide range of abnormalities including alterations in mitochondrial morphology, changes in ATP, and elevation of lactate levels. Further proof of the loss of gatekeeping function comes from analyzing animals bearing the MICU1$^{-/-}$EMRE$^{+/-}$ genotype. When compared to MICU1$^{-/-}$ mitochondria, the mitochondria derived from these animals have reduced EMRE expression and slower rates of calcium uptake at both low and high extra-mitochondrial calcium concentrations. Thus, in the setting of MICU1 deletion, deletion of one allele of EMRE appears to restrict uniporter opening, thereby helping to prevent MICU1-induced calcium overload. The observation that EMRE heterozygosity also markedly improves the overall survival of MICU1$^{-/-}$ mice provides strong genetic proof that the primary *in vivo* function of MICU1 is to serve as a gatekeeper of the uniporter complex.

Our data suggest that MICU1 is not required during embryogenesis. However, immediately after birth, the absence of MICU1 induces high rates of perinatal mortality, with the majority of MICU1$^{-/-}$ mice dying in the first 48 hours. Indeed, based on a large number of births from four independent founder lines, we estimate that in a C57BL/6N background, only one in six to seven MICU1$^{-/-}$ mice survive beyond one week. In contrast, while this manuscript was under review, another group reported that MICU1 deletion resulted in complete perinatal mortality (Antony et al., 2016). These survival differences might relate to subtle differences in the animal facilities, or more likely to the known mitochondrial differences between C57BL/6J and C57BL/6N sub-strains (Nicholson et al., 2010; Toye et al., 2005). Remarkably, our mice that do survive past one week function surprisingly well, and actually appear to improve with time. We have currently observed MICU1$^{-/-}$ mice up to a year of age, and the only additional phenotype that has emerged is the appearance of chorea-like movements (See Supplemental Movie 1), a feature seen in human patients as well (Logan et al., 2014). This would suggest that the absence of MICU1 expression is particularly critical immediately after birth. This may relate to the essential role of the mitochondria in the transition from the relatively hypoxic environment of the placenta to the oxygenated environment found after birth. We do not have a clear understanding as to why the functional defects in the surviving MICU1$^{-/-}$ mice seem most pronounced in skeletal muscle and the brain. In that regard, additional studies are needed to understand these tissue-specific effects. Comparisons of calcium uptake in different tissues, particularly between excitatory tissues such as skeletal muscle, brain and heart versus non-excitatory tissues such as liver and kidney might therefore be informative.

The gradual improvement of MICU1$^{-/-}$ mice over time perhaps suggests that mitochondria are capable of undergoing some level of functional remodeling. Such remodeling has been recently demonstrated in animal models in which MCU activity is reduced (Rasmussen et al., 2015) and may also explain the more pronounced phenotype in mouse models of acute MCU deletion in adult animals (Kwong et al., 2015; Luongo et al., 2015), when contrasted to models in which MCU is deleted or inhibited throughout embryogenesis (Holmstrom et al., 2015; Pan et al., 2013; Rasmussen et al., 2015). In the case of MICU1 deletion, this remodeling appears to involve alterations in the expression ratio of MCU to EMRE. It will be interesting to discern whether this remodeling represents some form of retrograde signaling from the mitochondria to the nucleus. There is increasing evidence of the importance of retrograde signaling whereby damaged or stress mitochondria emit a poorly characterized signal that elicits a protective nuclear response (Haynes et al., 2013). In that regard, it is of interest to note that some previous studies have implicated calcium as a mediator of the mammalian retrograde response (Biswas et al., 1999).

Finally, there is increasing realization that mitochondrial calcium overload might be a final common pathway in a multitude of disease conditions including various myopathies, certain neurodegenerative diseases, models of heart failure, and ischemic tissue injury (Abeti and Abramov, 2015; Bhosale et al., 2015; Martin and McGee, 2014; Santulli et al., 2015; Vallejo-Illarramendi et al., 2014). As such, strategies that modulate mitochondrial calcium uptake might have wide therapeutic potential. The demonstration here that modulating EMRE expression is capable of markedly improving the overall survival, as well as the biochemical, neurological, and myopathic phenotype of MICU1$^{-/-}$ mice, suggests that efforts to modulate the uniporter complex might be an effective therapeutic avenue for the growing number of disease states characterized by calcium overload.

Experimental Procedures

Generation of MICU1 and EMRE knockout mice by the CRISPR/Cas9 method

The MICU1 and EMRE knockout mice were generated using the CRISPR/Cas9 method as previously reported (Wang et al., 2013). Briefly, two single guide RNAs (sgRNAs) were designed to target each gene, one near the translation initiation codon (ATG) and the other one further downstream within the same exon. Specifically, the nucleotide sequences for these sgNRAs were: MICU1-sgRNA 1: TGTTAAGACGAAACATCCTG (reverse orientation); MICU1-sgRNA 2: TCTGCAGTGACTGCAAGTAC; EMRE-sgRNA 1: GGAGCTGGAGATGGCGTCCA; and EMRE-sgRNA 2: GCCTGGGTTGCAGTTCGACC. These sequences were cloned into a sgRNA vector using OriGene's gRNA Cloning Services (Rockville, Maryland), and were then used as templates to synthesize sgRNAs using the MEGAshortscript T7 Kit (Life Technologies). Cas9 mRNA was *in vitro* transcribed from plasmid MLM3613 (Addgene #42251) using the mMESSAGE mMACHINE T7 Ultra Kit (Life Technologies). For microinjection, Cas9 mRNA (100ng/μL) was mixed with either one or both sgRNA(s) for each gene (20ng/μL each sgRNA) and then microinjected into the cytoplasm of fertilized eggs collected from either C57BL/6N inbred (MICU1) or B6CBAF1/J F1 (EMRE) hybrid mice. The injected zygotes were cultured overnight in M16 medium at 37°C in 5% CO_2. The next morning, those embryos that had reached 2-cell stage

of development were implanted into the oviducts of pseudopregnant foster mothers (Swiss Webster, Taconic Farm). The mice born to the foster mothers were genotyped using PCR and DNA sequencing.

Mice

The MICU1 mice were maintained on a C57BL/6N or C57BL/6NxJ F1 background and experimental mice were obtained by breeding the mice using heterozygous crosses. Genotyping for MICU1 was performed using the following primers: 5'-CTGAGGCCAATTAACTGC-3' (forward) and 5'-GACACGACTAGCTGATAAACCT-3' (reverse). MICU1 heterozygous mice were bred to EMRE heterozygous mice (B6CBAF1/J x CD-1 or C57BL/6N) to generate double heterozygous breeders. Genotyping for EMRE was performed using the following primers: 5'-ACCGGCATACGAATGCGTGCTC-3' (forward) and 5'-ACCGGCCTCAATCCCTTCGTC-3' (reverse). All animal studies were done in accordance and approval of the NHLBI Animal Care and Use Committee.

Cell culture

Mouse embryonic fibroblasts (MEFs) were prepared using standard methods from E12–E14 day old embryos resulting from MICU1 heterozygous breeders. MEFs were cultured in growth medium consisting of Dulbecco's Modified Eagle's medium (DMEM; Invitrogen) supplemented with 15% fetal bovine serum (FBS), 50 U/ml penicillin and 50 μg/ml streptomycin. An epitope-tagged expression vector encoding MICU1 was generated using a C-terminal FLAG epitope in-frame with MICU1 derived from wild-type MEF cDNA. The construct was inserted into pCMV-Tag 4A (Stratagene) using the following primers: 5'-CGC GGA TCC ATG TTT CGT CTT AAC ACC CTT TCT GCG-3' and 5'-GCA TGT GAT ATC TTT GGG CAG AGC AAA GTC CCA GGC-3'. The construct was then inserted into the lentiviral expression vector pLVX-puro (Clontech) by using the following primers: 5'-TAG AAT TAT CTA GAG TCG CGG GAT CCG ACT CAC TAT AGG GCG AAT TGG G-3' and 5'-CAG ATC TCG AGC TCA AGC TTC GAT TAA CCC TCA CTA AAG GGA ACA AAA GC-3'. Lentivirus were produced in 293T cells and concentrated by ultracentrifugation by standard methods. MEFs were infected with lentivirus expressing epitope-tagged MICU1 or empty pLVX vector at an estimated MOI of 0.5 and subsequently selected with puromycin. All constructs were verified by DNA sequencing.

Mitochondrial isolation

Mitochondria were isolated by standard differential centrifugation protocol. Tissues were first minced in isolation buffer (225 mM mannitol, 75 mM sucrose, 5 mM MOPS, 0.5 mM EGTA, 2 mM taurine, pH adjusted to 7.25) then homogenized using a Glas-Col homogenizer at 1800 rpm for 8 to 12 strokes. The mixture was centrifuged for 5 minutes at 500 × g, and the supernatant was removed and centrifuged again. The supernatant was then centrifuged at 11,000 × g for 5 min to pellet the mitochondria, which were washed once more with isolation buffer and resuspended. Protein content was measured using a BCA protein assay (Thermo Scientific).

Intra-mitochondrial calcium levels

Measurement of mitochondrial Ca^{2+} content was performed as previously described, with minor adjustment as delineated below (Pan et al., 2013) In brief, brain mitochondria were isolated as described above in the presence of 3 μM Ru360 (Calbiochem) and washed in isolation buffer without EGTA. Mitochondria were pelleted and diluted in 0.6 N HCl, homogenized, and sonicated. Samples were heated for 30 min at 95 °C and then centrifuged for 5 min at 10,000*g*. The supernatants were recovered and the Ca^{2+} content in the supernatants was determined spectrophotometrically using the *O*-Cresolphthalein Complexone calcium assay kit (Cayman Chemical). Only samples that fell within the range of the standard curve were included for analysis and all values were normalized to the calcium levels observed in WT mitochondria.

Calcium uptake assay

Calcium uptake in mitochondria and MEFs was assayed similarly to what has been previously described (Kamer and Mootha, 2014). Briefly, isolated mitochondria and MEFs were resuspended in a buffer containing 125 mM KCl, 2mM K_2HPO_4, 10 μM EGTA, 1 mM $MgCl_2$, 20 mM HEPES at pH 7.2, 5 mM glutamate, and 5 mM malate. For MEFs, 0.004% digitonin was added to permeabilize the cells. The fluorescent cell-impermeable Ca^{2+} indicator Fluo4 (high-affinity, used for low extra-mitochondrial calcium conditions, final concentration 1 μM, Thermo Fisher) or Calcium Green-5N (low-affinity, used for high extra-mitochondrial conditions, final concentration 1 μM, Thermo Fisher) was added to the buffer. Fluorescence was measured at 506 nm excitation and 532 nm emission on an Omega plate reader. Experiments were initiated by injecting 5 μM or 25 μM $CaCl_2$, resulting in an approximate free calcium concentration of 0.5 μM or 16 μM free [Ca^{2+}], respectively. Calcium uptake curves were normalized to baseline and maximum, and relative rate of calcium uptake was calculated as the absolute value of the slope from linear regression fit in the linear range of the fluorescent signal (80 s to 300 s at low [Ca^{2+}] and 40 s to 110 s at high [Ca^{2+}]). Relative rates of calcium uptake were normalized to WT.

Supplementary Material

Refer to Web version on PubMed Central for supplementary material.

Acknowledgements

We are grateful to Michele Allen for help in mouse phenotyping, Erin Stempinski, Camron Keshavarz and Christopher Bleck for help with electron microscopic analysis, and Jeffrey Culver at Sanford-Burnham Orlando Metabolomics Core for skeletal muscle lactate measurements. This work was supported by Intramural NIH Funds and a Leducq Transatlantic Network grant (T.F.) and a PRAT postdoctoral fellowship from NIGMS (J.C.L.).

References

Abeti R, Abramov AY. Mitochondrial Ca(2+) in neurodegenerative disorders. Pharmacol Res. 2015; 99:377–381. [PubMed: 26013908]

Antony AN, Paillard M, Moffat C, Juskeviciute E, Correnti J, Bolon B, Rubin E, Csordas G, Seifert EL, Hoek JB, et al. MICU1 regulation of mitochondrial Ca(2+) uptake dictates survival and tissue regeneration. Nat Commun. 2016; 7:10955. [PubMed: 26956930]

Balaban RS. The role of Ca(2+) signaling in the coordination of mitochondrial ATP production with cardiac work. Biochimica et biophysica acta. 2009; 1787:1334–1341. [PubMed: 19481532]

Baughman JM, Perocchi F, Girgis HS, Plovanich M, Belcher-Timme CA, Sancak Y, Bao XR, Strittmatter L, Goldberger O, Bogorad RL, et al. Integrative genomics identifies MCU as an essential component of the mitochondrial calcium uniporter. Nature. 2011; 476:341–345. [PubMed: 21685886]

Bhosale G, Sharpe JA, Sundier SY, Duchen MR. Calcium signaling as a mediator of cell energy demand and a trigger to cell death. Ann N Y Acad Sci. 2015; 1350:107–116. [PubMed: 26375864]

Biswas G, Adebanjo OA, Freedman BD, Anandatheerthavarada HK, Vijayasarathy C, Zaidi M, Kotlikoff M, Avadhani NG. Retrograde Ca2+ signaling in C2C12 skeletal myocytes in response to mitochondrial genetic and metabolic stress: a novel mode of inter-organelle crosstalk. Embo J. 1999; 18:522–533. [PubMed: 9927412]

Bohm J, Chevessier F, Maues De Paula A, Koch C, Attarian S, Feger C, Hantai D, Laforet P, Ghorab K, Vallat JM, et al. Constitutive activation of the calcium sensor STIM1 causes tubular-aggregate myopathy. Am J Hum Genet. 2013; 92:271–278. [PubMed: 23332920]

Csordas G, Golenar T, Seifert EL, Kamer KJ, Sancak Y, Perocchi F, Moffat C, Weaver D, de la Fuente Perez S, Bogorad R, et al. MICU1 controls both the threshold and cooperative activation of the mitochondrial Ca(2)(+) uniporter. Cell metabolism. 2013; 17:976–987. [PubMed: 23747253]

Csordas G, Thomas AP, Hajnoczky G. Quasi-synaptic calcium signal transmission between endoplasmic reticulum and mitochondria. Embo J. 1999; 18:96–108. [PubMed: 9878054]

Csordas G, Varnai P, Golenar T, Roy S, Purkins G, Schneider TG, Balla T, Hajnoczky G. Imaging interorganelle contacts and local calcium dynamics at the ER-mitochondrial interface. Molecular cell. 2010; 39:121–132. [PubMed: 20603080]

de la Fuente S, Matesanz-Isabel J, Fonteriz RI, Montero M, Alvarez J. Dynamics of mitochondrial Ca2+ uptake in MICU1-knockdown cells. Biochem J. 2014; 458:33–40. [PubMed: 24313810]

De Stefani D, Raffaello A, Teardo E, Szabo I, Rizzuto R. A forty-kilodalton protein of the inner membrane is the mitochondrial calcium uniporter. Nature. 2011; 476:336–340. [PubMed: 21685888]

Deluca HF, Engstrom GW. Calcium uptake by rat kidney mitochondria. Proceedings of the National Academy of Sciences of the United States of America. 1961; 47:1744–1750. [PubMed: 13885269]

Fieni F, Lee SB, Jan YN, Kirichok Y. Activity of the mitochondrial calcium uniporter varies greatly between tissues. Nat Commun. 2012; 3:1317. [PubMed: 23271651]

Foskett JK, Philipson B. The mitochondrial Ca(2+) uniporter complex. J Mol Cell Cardiol. 2015; 78:3–8. [PubMed: 25463276]

Giacomello M, Drago I, Bortolozzi M, Scorzeto M, Gianelle A, Pizzo P, Pozzan T. Ca2+ hot spots on the mitochondrial surface are generated by Ca2+ mobilization from stores, but not by activation of store-operated Ca2+ channels. Molecular cell. 2010; 38:280–290. [PubMed: 20417605]

Haynes CM, Fiorese CJ, Lin YF. Evaluating and responding to mitochondrial dysfunction: the mitochondrial unfolded-protein response and beyond. Trends Cell Biol. 2013; 23:311–318. [PubMed: 23489877]

Holmstrom KM, Pan X, Liu JC, Menazza S, Liu J, Nguyen TT, Pan H, Parks RJ, Anderson S, Noguchi A, et al. Assessment of cardiac function in mice lacking the mitochondrial calcium uniporter. J Mol Cell Cardiol. 2015; 85:178–182. [PubMed: 26057074]

Kamer KJ, Mootha VK. MICU1 and MICU2 play nonredundant roles in the regulation of the mitochondrial calcium uniporter. EMBO Rep. 2014; 15:299–307. [PubMed: 24503055]

Kamer KJ, Mootha VK. The molecular era of the mitochondrial calcium uniporter. Nat Rev Mol Cell Biol. 2015; 16:545–553. [PubMed: 26285678]

Kirichok Y, Krapivinsky G, Clapham DE. The mitochondrial calcium uniporter is a highly selective ion channel. Nature. 2004; 427:360–364. [PubMed: 14737170]

Kovacs-Bogdan E, Sancak Y, Kamer KJ, Plovanich M, Jambhekar A, Huber RJ, Myre MA, Blower MD, Mootha VK. Reconstitution of the mitochondrial calcium uniporter in yeast. Proceedings of the National Academy of Sciences of the United States of America. 2014; 111:8985–8990. [PubMed: 24889638]

Kwong JQ, Lu X, Correll RN, Schwanekamp JA, Vagnozzi RJ, Sargent MA, York AJ, Zhang J, Bers DM, Molkentin JD. The Mitochondrial Calcium Uniporter Selectively Matches Metabolic Output to Acute Contractile Stress in the Heart. Cell Rep. 2015; 12:15–22. [PubMed: 26119742]

Logan CV, Szabadkai G, Sharpe JA, Parry DA, Torelli S, Childs AM, Kriek M, Phadke R, Johnson CA, Roberts NY, et al. Loss-of-function mutations in MICU1 cause a brain and muscle disorder linked to primary alterations in mitochondrial calcium signaling. Nat Genet. 2014; 46:188–193. [PubMed: 24336167]

Luongo TS, Lambert JP, Yuan A, Zhang X, Gross P, Song J, Shanmughapriya S, Gao E, Jain M, Houser SR, et al. The Mitochondrial Calcium Uniporter Matches Energetic Supply with Cardiac Workload during Stress and Modulates Permeability Transition. Cell Rep. 2015; 12:23–34. [PubMed: 26119731]

Mallilankaraman K, Doonan P, Cardenas C, Chandramoorthy HC, Muller M, Miller R, Hoffman NE, Gandhirajan RK, Molgo J, Birnbaum MJ, et al. MICU1 is an essential gatekeeper for MCU-mediated mitochondrial Ca(2+) uptake that regulates cell survival. Cell. 2012; 151:630–644. [PubMed: 23101630]

Martin SD, McGee SL. The role of mitochondria in the aetiology of insulin resistance and type 2 diabetes. Biochimica et biophysica acta. 2014; 1840:1303–1312. [PubMed: 24060748]

Murgia M, Rizzuto R. Molecular diversity and pleiotropic role of the mitochondrial calcium uniporter. Cell Calcium. 2015; 58:11–17. [PubMed: 26048007]

Nguyen TT, Oh SS, Weaver D, Lewandowska A, Maxfield D, Schuler MH, Smith NK, Macfarlane J, Saunders G, Palmer CA, et al. Loss of Miro1-directed mitochondrial movement results in a novel murine model for neuron disease. Proceedings of the National Academy of Sciences of the United States of America. 2014; 111:E3631–3640. [PubMed: 25136135]

Nicholson A, Reifsnyder PC, Malcolm RD, Lucas CA, MacGregor GR, Zhang W, Leiter EH. Diet-induced obesity in two C57BL/6 substrains with intact or mutant nicotinamide nucleotide transhydrogenase (Nnt) gene. Obesity (Silver Spring). 2010; 18:1902–1905. [PubMed: 20057372]

Orrenius S, Zhivotovsky B, Nicotera P. Regulation of cell death: the calcium-apoptosis link. Nat Rev Mol Cell Biol. 2003; 4:552–565. [PubMed: 12838338]

Pan X, Liu J, Nguyen T, Liu C, Sun J, Teng Y, Fergusson MM, Rovira II, Allen M, Springer DA, et al. The physiological role of mitochondrial calcium revealed by mice lacking the mitochondrial calcium uniporter. Nature cell biology. 2013; 15:1464–1472. [PubMed: 24212091]

Patron M, Checchetto V, Raffaello A, Teardo E, Vecellio Reane D, Mantoan M, Granatiero V, Szabo I, De Stefani D, Rizzuto R. MICU1 and MICU2 finely tune the mitochondrial Ca2+ uniporter by exerting opposite effects on MCU activity. Molecular cell. 2014; 53:726–737. [PubMed: 24560927]

Peng TI, Jou MJ. Oxidative stress caused by mitochondrial calcium overload. Ann N Y Acad Sci. 2010; 1201:183–188. [PubMed: 20649555]

Perocchi F, Gohil VM, Girgis HS, Bao XR, McCombs JE, Palmer AE, Mootha VK. MICU1 encodes a mitochondrial EF hand protein required for Ca(2+) uptake. Nature. 2010; 467:291–296. [PubMed: 20693986]

Plovanich M, Bogorad RL, Sancak Y, Kamer KJ, Strittmatter L, Li AA, Girgis HS, Kuchimanchi S, De Groot J, Speciner L, et al. MICU2, a paralog of MICU1, resides within the mitochondrial uniporter complex to regulate calcium handling. PLoS One. 2013; 8:e55785. [PubMed: 23409044]

Raffaello A, De Stefani D, Sabbadin D, Teardo E, Merli G, Picard A, Checchetto V, Moro S, Szabo I, Rizzuto R. The mitochondrial calcium uniporter is a multimer that can include a dominant-negative pore-forming subunit. Embo J. 2013; 32:2362–2376. [PubMed: 23900286]

Rasmussen TP, Wu Y, Joiner ML, Koval OM, Wilson NR, Luczak ED, Wang Q, Chen B, Gao Z, Zhu Z, et al. Inhibition of MCU forces extramitochondrial adaptations governing physiological and pathological stress responses in heart. Proceedings of the National Academy of Sciences of the United States of America. 2015; 112:9129–9134. [PubMed: 26153425]

Rizzuto R, Pinton P, Carrington W, Fay FS, Fogarty KE, Lifshitz LM, Tuft RA, Pozzan T. Close contacts with the endoplasmic reticulum as determinants of mitochondrial Ca2+ responses. Science. 1998; 280:1763–1766. [PubMed: 9624056]

Sancak Y, Markhard AL, Kitami T, Kovacs-Bogdan E, Kamer KJ, Udeshi ND, Carr SA, Chaudhuri D, Clapham DE, Li AA, et al. EMRE is an essential component of the mitochondrial calcium uniporter complex. Science. 2013; 342:1379–1382. [PubMed: 24231807]

Santulli G, Xie W, Reiken SR, Marks AR. Mitochondrial calcium overload is a key determinant in heart failure. Proceedings of the National Academy of Sciences of the United States of America. 2015; 112:11389–11394. [PubMed: 26217001]

Toye AA, Lippiat JD, Proks P, Shimomura K, Bentley L, Hugill A, Mijat V, Goldsworthy M, Moir L, Haynes A, et al. A genetic and physiological study of impaired glucose homeostasis control in C57BL/6J mice. Diabetologia. 2005; 48:675–686. [PubMed: 15729571]

Vais H, Mallilankaraman K, Mak DO, Hoff H, Payne R, Tanis JE, Foskett JK. EMRE Is a Matrix Ca(2+) Sensor that Governs Gatekeeping of the Mitochondrial Ca(2+) Uniporter. Cell Rep. 2016; 14:403–410. [PubMed: 26774479]

Vallejo-Illarramendi A, Toral-Ojeda I, Aldanondo G, Lopez de Munain A. Dysregulation of calcium homeostasis in muscular dystrophies. Expert Rev Mol Med. 2014; 16:e16. [PubMed: 25293420]

Vasington FD, Murphy JV. Ca ion uptake by rat kidney mitochondria and its dependence on respiration and phosphorylation. J Biol Chem. 1962; 237:2670–2677. [PubMed: 13925019]

Wang H, Yang H, Shivalila CS, Dawlaty MM, Cheng AW, Zhang F, Jaenisch R. One-step generation of mice carrying mutations in multiple genes by CRISPR/Cas-mediated genome engineering. Cell. 2013; 153:910–918. [PubMed: 23643243]

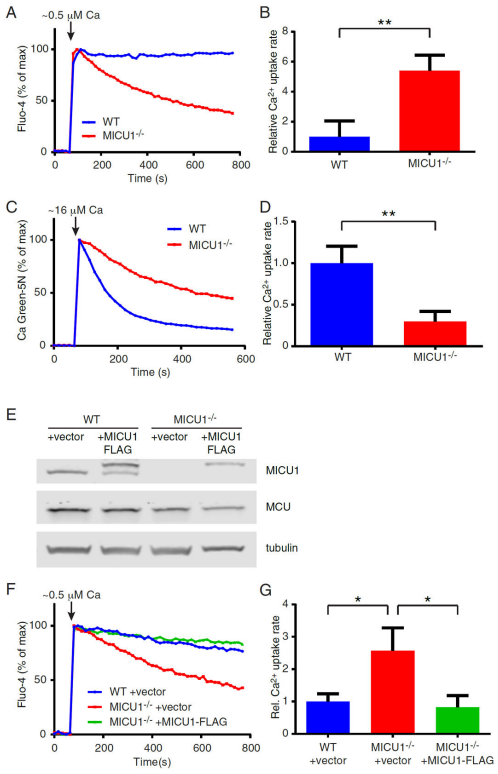

Figure 1.

MICU1 regulates calcium uptake. **A**) Representative extra-mitochondrial calcium traces with WT or MICU1$^{-/-}$ liver mitochondria using the calcium indicator Fluo-4. Estimated free calcium concentration is 0.5 μM. **B**) Quantification of calcium uptake rates in liver mitochondria at low (0.5 μM) extra-mitochondrial calcium concentration (n=5 per genotype; data is represented as mean +/− SD). **C**) Representative extra-mitochondrial calcium traces with WT or MICU1$^{-/-}$ liver mitochondria at high calcium concentration (estimated at 16 μM) using Calcium Green-5N as an indicator. **D**) Quantification of calcium uptake rates in liver mitochondria at high (16 μM) extra-mitochondrial calcium concentration (n=5 per genotype; data is represented as mean +/− SD). **E**) Western blot of MEFs isolated from WT and MICU1$^{-/-}$ embryos that were stably transduced with either an empty vector, or with a vector encoding an epitope-tagged MICU1 construct. Protein levels of MICU1, MCU, and tubulin as a loading control are shown. **F**) Representative traces of cytosolic calcium measurements in permeabilized cells exposed to a pulse of approximately 0.5 μM free calcium. Shown are WT MEFs infected with a vector control, MICU1$^{-/-}$ MEFs with a vector control, or MICU1$^{-/-}$ MEFs reconstituted with a lentivirus encoding an epitope-tagged MICU1. **G**) Quantification of calcium uptake rates at low calcium concentration (0.5 μM) in permeabilized MEFs (n=3 per condition; mean +/− SD). **p<0.01, *p<0.05 See also Figure S1.

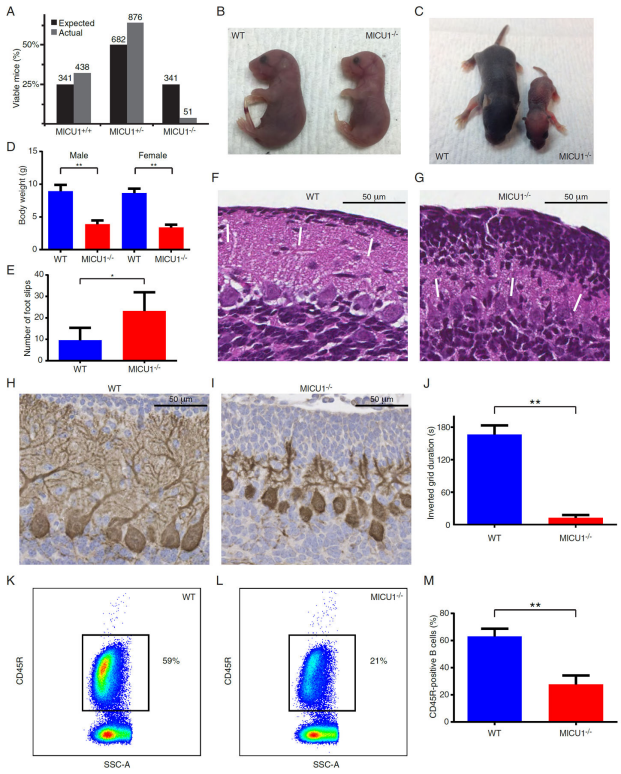

Figure 2.

Mice lacking MICU1 develop multiple neurologic and myopathic defects. **A**) Expected and observed number of MICU1$^{+/+}$, MICU1$^{+/-}$, and MICU1$^{-/-}$ mice surviving over one week. Actual number of expected and observed mice is shown above each bar from a total of over 1300 offspring. **B**) E20 littermates demonstrating the appearance of a WT and slightly smaller MICU1$^{-/-}$ embryo. **C**) Appearance of WT and MICU1$^{-/-}$ mice at 1 week of age. **D**) Body weight for 14- to 18-day-old male (n=12) and female (n=6) WT and MICU1$^{-/-}$ mice. Data is represented as mean +/− SD. **E**) Cerebellar function in 4-week-old WT and MICU1$^{-/-}$ mice assessed by performance on a balance beam and measured as cumulative number of foot slips (n=4 mice per genotype; mean +/− SD). **F**) Cerebellar architecture in 12-day-old WT mice or **G**) MICU1$^{-/-}$ mice. Arrows denote outer granular layer. **H**) Calbindin staining demonstrating Purkinje cell morphology in 12-day-old WT and **I**) MICU1$^{-/-}$ cerebellum. **J**) Assessment of muscle strength using an inverted grid test at 4 weeks of age (n=4 mice per genotype; mean +/− SD). **K**) Representative FACS-based assessment of splenic B cell (CD45R^{+}) abundance in WT and **L**) MICU1$^{-/-}$ mice (SSC-A; side scatter area). **M**) Mean B cell percentage in spleens of 2- to 3-week-old WT and MICU1$^{-/-}$ mice (n=6 per genotype; mean +/− SD). **p<0.01, *p<0.05 See also Figures S2 and S3.

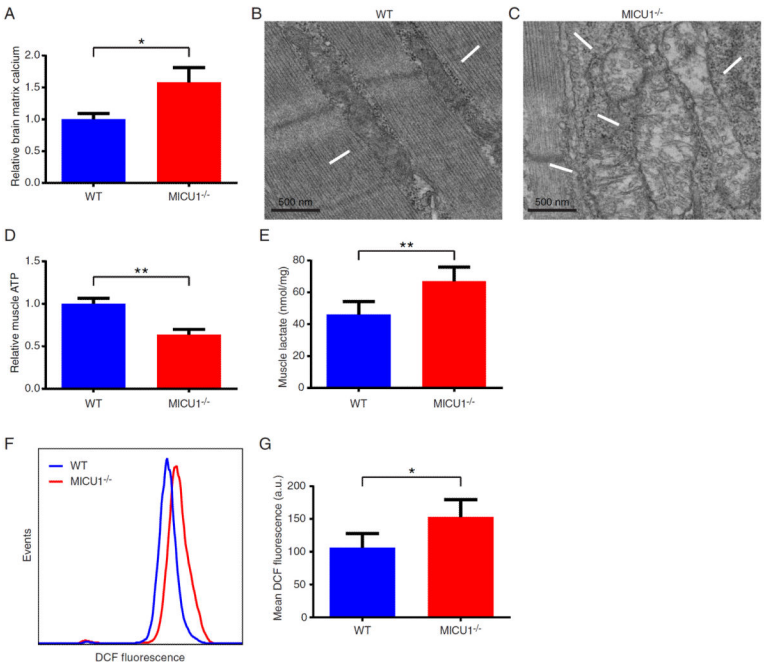

Figure 3.

MICU1-deficient mice develop mitochondrial defects. **A**) Relative levels of mitochondrial matrix calcium in WT and MICU1$^{-/-}$ mice. Mitochondria were isolated from the brains of 14- to 18-day-old mice (n=3 per genotype; mean +/− SD). **B**) Electron micrograph of WT and **C**) MICU1$^{-/-}$ skeletal muscle at 9 days of age. Arrows indicate mitochondria. **D**) Relative skeletal muscle ATP levels in 14- to 18-day-old WT and MICU1$^{-/-}$ mice (n=5 mice per genotype; mean +/−SD). **E**) Skeletal muscle lactate levels in 12- to 16-day-old WT and MICU1$^{-/-}$ mice (n=5 mice per genotype; mean +/− SD). **F**) Representative levels of ROS as assessed by DCF fluorescence in IgM-positive B cells from WT and MICU1$^{-/-}$ mice. **G**) Mean DCF fluorescent intensity in IgM-positive B cells obtained from 2- to 3-week-old WT and MICU1$^{-/-}$ mice (n=5 per genotype; mean +/− SD). **p<0.01, *p<0.05 See also Figure S4.

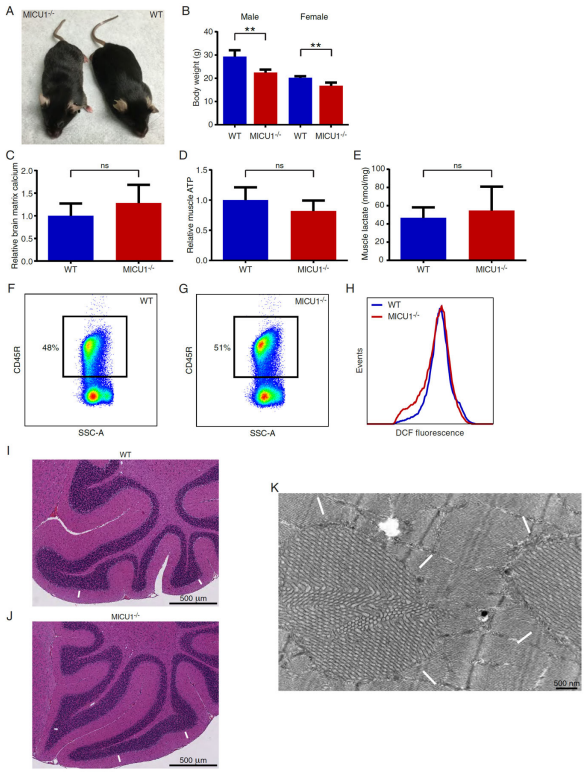

Figure 4.

Surviving MICU1-deficient mice improve over time. **A**) Appearance of WT and MICU1$^{-/-}$ mice at 8 months of age. **B**) Body weight of 3–4 month old male and female WT and MICU1$^{-/-}$ mice (n=7 WT male and n=4 WT female; n=9 MICU1$^{-/-}$ male and n=4 MICU1$^{-/-}$ female mice). Data is represented as mean +/− SD. **C**) Relative levels of mitochondrial matrix calcium in WT and MICU1$^{-/-}$ mice. Mitochondria were isolated from the brains of 7-month-old mice (n=6 per genotype; mean +/− SD). **D**) Relative skeletal muscle ATP levels in 7-month-old WT and MICU1$^{-/-}$ mice (n=5 mice per genotype; mean +/−SD). **E**) Skeletal muscle lactate levels in 7-month-old WT and MICU1$^{-/-}$ mice (n=5 mice per genotype; mean +/− SD). **F**) Representative FACS-based assessment of splenic B cell (CD45R^{+}) abundance in 7-month-old WT and **G**) MICU1$^{-/-}$ mice (SSC-A; side scatter area). **H**) Representative levels of ROS as assessed by DCF fluorescence in IgM-positive B cells from 7-month-old WT and MICU1$^{-/-}$ mice. **I**) Cerebellar architecture in 6-week-old WT mice or **J**) MICU1$^{-/-}$ mice. Arrows indicate normal appearing outer granular layer. **K**) Electron micrograph of MICU1$^{-/-}$ skeletal muscle at 7 months of age. Arrows indicate tubular aggregates. **p<0.01, *p<0.05 See also Figure S5.

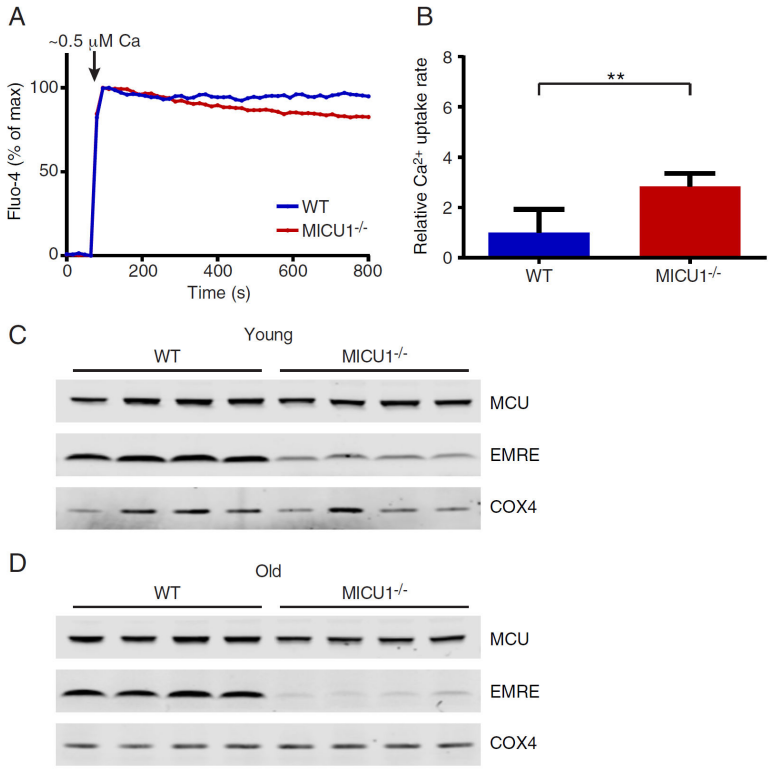

Figure 5.

Older MICU1-deficient mice exhibit improved calcium uptake and reduced EMRE expression. **A**) Representative extra-mitochondrial calcium traces with WT or MICU1$^{-/-}$ liver mitochondria from 7-month-old mice using the calcium indicator Fluo-4. Estimated free calcium concentration is 0.5 μM. **B**) Quantification of calcium uptake rates in liver mitochondria from 7-month-old mice at low (0.5 μM) extra-mitochondrial calcium concentration (n=3 per genotype; data is represented as mean +/− SD). **C**) Western blot of MCU and EMRE protein levels in liver mitochondria obtained from four pairs of 2-week-old WT and MICU1$^{-/-}$ mice. **D**) Western blot of MCU and EMRE protein levels in liver mitochondria obtained from four pairs of 7-month-old WT and MICU1$^{-/-}$ mice. The mitochondrial protein COX4 is shown as a loading control.

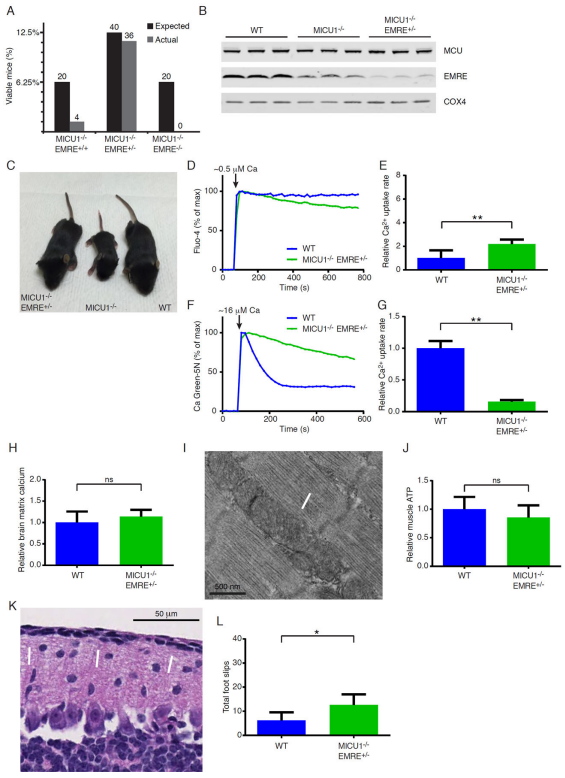

Figure 6.

EMRE heterozygosity ameliorates MICU1 deficiency. **A**) Percentage of observed and expected MICU1-deficient mice surviving past one week with either $EMRE^{+/+}$, $EMRE^{+/-}$, and $EMRE^{-/-}$ genotype status. Actual number of expected and observed mice from $MICU1^{+/-}EMRE^{+/-}$ crosses is shown above each bar. **B**) Western blot of MCU and EMRE protein levels in liver mitochondria obtained from 2-week-old WT, $MICU1^{-/-}$, and $MICU1^{-/-}EMRE^{+/-}$ mice. The mitochondrial protein COX4 is shown as a loading control. **C**) Appearance of 14-day-old WT, $MICU1^{-/-}$ and $MICU1^{-/-}EMRE^{+/-}$ mice. **D**) Representative extra-mitochondrial calcium traces for WT and $MICU1^{-/-}EMRE^{+/-}$ liver mitochondria using the calcium indicator Fluo-4. Estimated free calcium concentration is 0.5 μM. **E**) Quantification of calcium uptake rates in WT (n=5) and $MICU1^{-/-}EMRE^{+/-}$ liver mitochondria (n=7) at low calcium concentration (0.5 μM). Data is represented as mean +/− SD. **F**) Representative extra-mitochondrial calcium traces for WT and $MICU1^{-/-}EMRE^{+/-}$ liver mitochondria using the calcium indicator Calcium Green-5N. Approximate free calcium concentration is 16 μM. **G**) Quantification (mean+/−SD) of calcium uptake rates in WT (n=5) and $MICU1^{-/-}EMRE^{+/-}$ liver mitochondria (n=7) at high calcium concentration (16 μM). **H**) Relative matrix calcium levels in mitochondria isolated from the brain of 2- to 3-week-old WT (n=6) and $MICU1^{-/-}EMRE^{+/-}$ (n=6) mice (mean +/−SD). **I**) Electron micrograph of skeletal muscle in a 17-day-old $MICU1^{-/-}EMRE^{+/-}$ mouse. Arrows indicate normal-appearing mitochondria. **J**) Relative ATP levels in the skeletal muscle of 2–3 week old WT (n=7) and $MICU1^{-/-}EMRE^{+/-}$ (n=10) mice (mean +/− SD). **K**) Cerebellar histology of 16-day-old $MICU1^{-/-}EMRE^{+/-}$ mice. Arrows indicate normal appearing outer granular layer. **L**) Cerebellar function in 4-week-old WT and $MICU1^{-/-}EMRE^{+/-}$ mice assessed by

performance on a balance beam and measured as cumulative number of foot slips (n=4 mice per genotype; mean +/− SD). **p<0.01, *p<0.05 See also Figure S6.